



Atmospheric icing on large wind turbine blades

Muhammad S. Virk¹, Matthew C. Homola², Per J. Nicklasson¹

¹ Department of Technology, Narvik University College, 8505 Narvik, Norway.

² Nordkraft Produksjon, Narvik, Norway.

Abstract

A numerical study of atmospheric ice accretion on a large horizontal axis 'NREL 5 MW' wind turbine blade has been carried out using the computational fluid dynamics based technique. Numerical analyses were carried out at five different sections along the wind turbine blade for both rime and glaze ice conditions. Based upon the flow field calculation and the droplet collision efficiency, the rate and shape of accreted ice was simulated at different atmospheric temperatures. Results indicate that the icing is less severe near the blade root sections, where the blade profiles are larger and thicker, both in terms of local ice mass and accreted ice thickness. Change in accreted ice growth with the atmospheric temperature is significant along the blade sections from centre to tip. The research work also highlighted that the ice accretion on wind turbine blades can also be controlled by optimizing its geometric design features instead of only using the energy consuming anti icing and de-icing systems.

Copyright © 2012 International Energy and Environment Foundation - All rights reserved.

Keywords: Wind turbine blade; Atmospheric icing; CFD; Atmospheric temperature.

1. Introduction

Wind energy is a widely accepted source of power available every where in the world. Its a reliable alternative energy source, which is not depleted over time. Most northern regions of the world like arctic and alpine regions have good wind resources, but icing on wind turbines has been recognized as a hindrance to the development of the wind power in these regions[1]. A variety of problems due to icing on wind turbines have been documented including complete loss of power production [2], reduction of power due to the disrupted aerodynamics, overloading due to delayed stall, increased fatigue of components due to imbalance in the ice load [3] and damage or harm caused by the uncontrolled shedding of large ice chunks [4]. Annual power losses due to ice accretion on the wind turbine blades, at some sites subject to icing rate, are estimated to be about 20% [5].

Ice accretion on the wind turbine blades is caused by the impingement of super cooled water droplets. Most of these liquid water droplets freeze immediately upon impact due to rapid heat dissipation leading to ice accretion. The location and intensity of water impingement can be numerically determined by solving the air-water multiphase flow in proximity of the blade. The shape of the accreted ice depends upon many variables such as point of operation, the geometry of wind turbine blade, relative wind velocity, temperature, droplet diameter and the liquid water content [6]. Atmospheric icing on the wind turbine blades has been numerically simulated for a variety of cases in the past [3, 7-9]. In this paper computational fluid dynamics based three dimensional numerical analyses were carried out to study the rate and shape of ice growth on a large wind turbine blade. NREL 5MW wind turbine blade [10] was selected as test case for this study, mainly because of its geometric size and the availability of test data.

Analyses were carried out at different atmospheric icing temperatures. Main objective of this study was to simulate the atmospheric ice along a large wind turbine blade and analyses the ice distribution to identify the most affected areas due to icing.

2. Numerical setup

The NREL 5 MW wind turbine's blade radius used for this study was 63 meters, therefore it was not possible to numerically simulate the icing on the whole blade due to limited computational resources. Therefore five sections were selected along the blade radius, where each section was 0.5 meter long (Figure 1). The selection of the tested sections was weighted towards the outer portion of the blade, as previous works has shown more ice on the outer half of the wind turbine blade [11, 12]. Analyses were carried out at different atmospheric temperatures and time intervals to study the rate and shape of ice growth for each section. These numerical analyses were carried out using an ice accretion solver 'FENSAP-ICE' from NTI [13]. Each selected section along the blade has different geometric characteristics (chord length, twist angle, thickness to chord ratio). Table 1 show the geometric characteristics of the complete blade, where the highlighted sections were used for these analyses.

Table 1. Distributed NREL 5 MW wind turbine's blade geometric properties; Source [10]

Node	Blade Radial Location (m)	Chord Length (m)	Aerodynamic Twist (degree)	Airfoil Table
1	4.3667	3.542	13.308	Cylinder
2	7.1	3.854	13.308	Cylinder
3	9.833	4.167	13.308	Cylinder
A 4	13.25	4.557	13.308	DU 40
5	17.35	4.652	11.480	DU 35
6	21.45	4.458	10.162	DU 35
7	25.55	4.249	9.011	DU 30
8	29.65	4.007	7.795	DU 25
B 9	33.75	3.748	6.544	DU 25
10	37.85	3.502	5.361	DU 21
C 11	41.95	3.256	4.188	DU 21
12	46.05	3.010	3.125	NACA 64618
13	40.15	2.764	2.319	NACA 64618
D 14	54.25	2.518	1.526	NACA 64618
15	57.66	2.313	0.863	NACA 64618
16	60.4	2.086	0.370	NACA 64618
E 17	63.13	1.419	0.106	NACA 64618

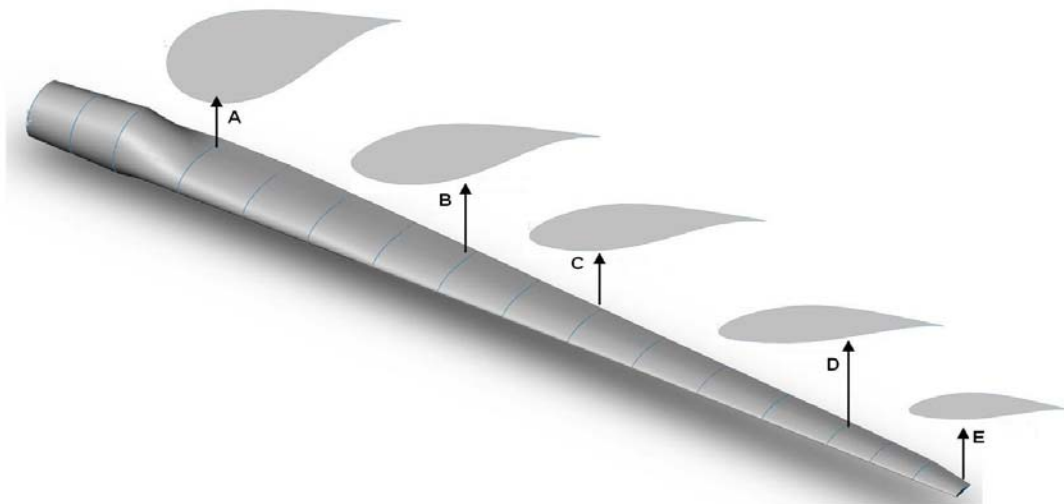


Figure 1. 3D CAD of the NREL 5 MW wind turbine blade, showing the selected sections

Each numerical simulation included two major parameters, the relative wind speed (V_{rel}) and the angle of attack (α). These parameters depend upon the free stream wind speed (V_{∞}), the axial and tangential induction factors (a and \tilde{a}), the simulated section's radius (r), the local speed ratio (λ_r) and the blade twist angle (ϕ) at that section. The relative wind speed and angle of attack at each section is calculated by ;

$$V_{rel} = \sqrt{(V_{\infty}(1-a))^2 + \left(\frac{\lambda_r r}{V_{\infty}}\right)^2} \quad (1)$$

$$\alpha = \arctan\left(\frac{1-a}{\lambda_r(1+\tilde{a})}\right) - \phi$$

And the local speed ratio was calculated by;

$$\lambda_r = \frac{\lambda r}{R} \quad (2)$$

where R is the rotor radius. The axial and tangential induction factors were iteratively calculated using the blade element momentum theory without tip loss corrections and assuming $C_d = 0$, with the following equations [14], where σ_r is the local solidity and $\beta = 90 - \alpha - \phi$ is the angle of the relative wind.

$$a = \frac{1}{\left(1 + \frac{4 \cos^2 \beta}{\sigma_r C_l \sin \beta}\right)} \quad (3)$$

$$\tilde{a} = \frac{\sigma_r C_l}{4 \lambda_r \cos \beta} (1-a)$$

Blade element momentum theory (BEM) is commonly used in analysis of wind turbine rotors and is based on the principal that the forces exerted on the rotor must be reflected in a change in momentum of the air passing through the rotor. The aerodynamic lift coefficients used for the BEM method were obtained from the tables published by NREL [15]

All the analyses were carried out at a free stream velocity ' V_{∞} ' of 10 m/sec, and blade tip speed ratio (λ) of 7.55. Table 2 shows the values of axial induction factors, relative wind speeds and the angle of attacks at each selected section along the blade used for this study.

Table 2. Test sections operating conditions

Blade Section	Blade Radius (m)	Relative Wind Velocity (m/sec)	Angle of Attack (degree)	Axial Induction Factor (a)
A	13.25	17.36	9.0	0.2969
B	33.75	41.07	3.5	0.2766
C	41.95	50.7	3.3	0.3317
D	54.25	65.33	4.3	0.3303
E	63.13	75.88	5.8	0.2134

C-type structured numerical grid was used for each section, whereas to accurately determine the boundary layer characteristics (shear stresses and heat fluxes), a y^+ value less than 1 was used near the wall. The blade profiles roughness height was calculated according to Shin, et al. [16]. The air flow around the wind turbine is typically turbulent at high Reynolds numbers. The one equation Spalart Allmaras turbulence model was used as a compromise between acceptable computational cost and the required accuracy in simulating the turbulent flow. The two phase flow was solved using Eulerian-Eulerian approach in FENSAP-ICE. The main advantage of using Eulerian-Eulerian approach is that, the same mesh can be used for multiphase flow calculations and ice geometry. The Messinger model of heat

transfer was used for the surface thermodynamics of the blade. All the numerical simulations were carried out at the operating conditions specified in Table 3.

Table 3. Operating conditions used for the simulations

Free Stream Wind Velocity [m/s]	10
Droplet Sizes , MVD [μm]	20
Liquid Water Content , LWC [g/m^3]	0.22
Atmospheric Air Temperatures [$^{\circ}\text{C}$]	-2.5, -5, -10, -15
Simulation Time [minutes]	60,180

3. Results & discussion

3.1 Flow behaviour & droplet distribution

Numerical analyses of the air flow behaviour show a change in the velocity and pressure distribution along each selected section of the wind turbine blade. Change of geometric characteristics at each section from blade tip to root leads to change in the relative velocity and angle of attack (Table 2) that effectively changes the flow behaviour along each section. Such change in the blade geometric characteristics is generally to avoid the stall of the blade root section. High flow separation is observed at root section (Section A) as compared to the blade centre section (Section C) and tip section (Section E). Liquid water droplet moving in the air stream is generally influenced by its drag and inertia, when neglecting the gravity and buoyancy [17]. If drag dominates the inertia the droplet follows the stream line whereas for the case where inertia dominates the particle hits the object. The ratio of inertia to drag depends upon the droplet size, velocity of air stream and dimensions of the object in question. Therefore with an increase in blade size (chord length) more droplets and especially the small droplets, move along the streamlines around the blade. As the blade sections near the root have larger chord length and thickness, results show low droplet collision efficiency near the root section of the blade, while a high value of droplet collision efficiency is observed near the tip section. This trend is strengthened by changes in relative velocity. Lower relative velocity nearer the blade root reduces the influence of the inertial component of droplet motion and also allows more droplets to follow the streamlines around the blade. Figure 2 shows the droplet collision efficiency at three different sections of the wind turbine blade.

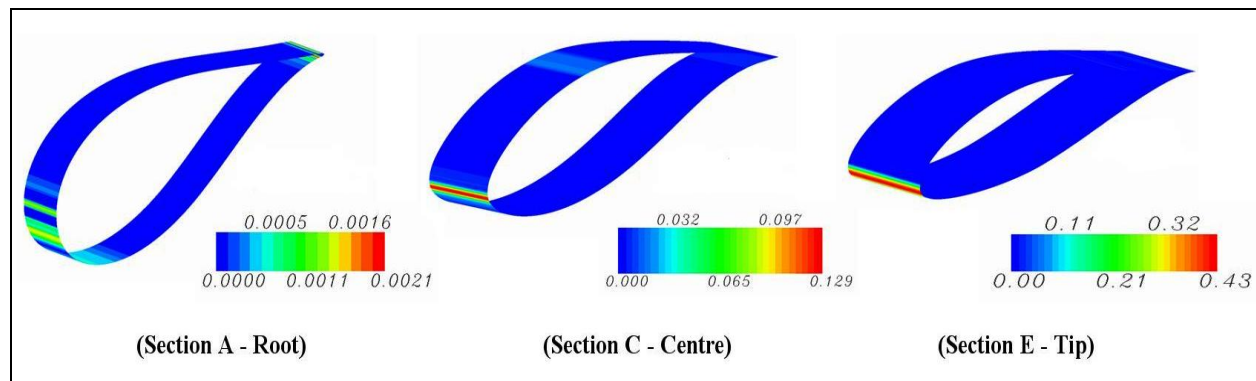


Figure 2. Droplet collision efficiency at different sections of NREL 5 MW wind turbine blade

3.2 Atmospheric ice accretion

To study the rate and shape of ice accretion at different sections along the wind turbine blade, the numerical analyses were carried out for $t = 60$ minutes. Results show a decrease in ice accretion that with the increase of blade profile size. Such decrease is mainly due to the decrease in collision efficiency of the droplets with the blade surface and the reduction in velocity. Section E, which is near the blade tip, has a smaller chord and blade thickness ratio, as well as a higher velocity, therefore more ice accretion was found at this section, whereas results show a gradual decrease in ice accretion, when moving towards the root section of the blade. Figure 3 shows the simulated ice accretion at three different sections of the blade at constant atmospheric temperature of, $T = -2.5^{\circ}\text{C}$ for $t = 60$ min.

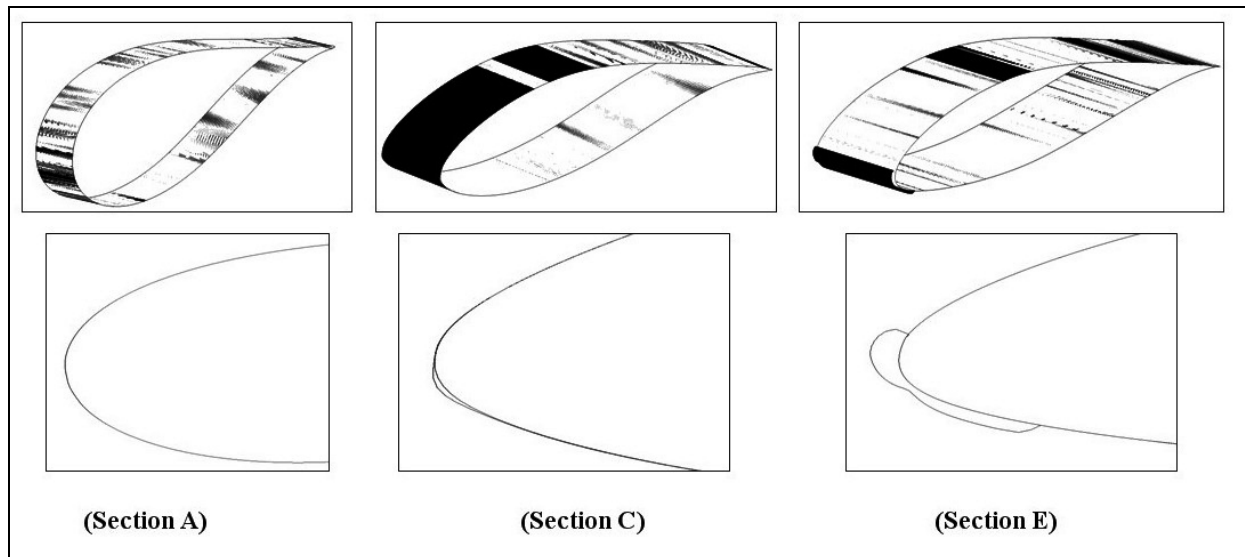


Figure 3. Rate and shape of ice accretion at different section of the NREL 5 MW wind turbine blade at $T = -2.5\text{ }^{\circ}\text{C}$, (black shaded area in the figure is the area covered by the ice), $t = 60\text{ min}$

In Figure 3, a significant difference in ice growth can be seen between section E (blade tip) and section C (blade centre). Although the area covered by the ice on section C is larger, the ice layer at section C is very thin, while at section E the accreted ice is considerably thicker as compared to section C. As mentioned above, with the increase of blade profile size the super cooled water droplets follow the stream line and their collision efficiency reduces which leads to decrease in rate of ice growth at these sections. As section C has a larger chord and blade thickness therefore more water droplets follow the streamline at this section and do not hit the blade section. Whereas at section E, due to smaller profile size the collision efficiency of the droplet is high and more ice accretion is observed at this section. To study the effect of atmospheric temperature variations on ice accretion, numerical analyses were carried out at four different temperatures ($-2.5\text{ }^{\circ}\text{C}$, $-5\text{ }^{\circ}\text{C}$, $-10\text{ }^{\circ}\text{C}$ and $-15\text{ }^{\circ}\text{C}$), assuming a constant median volume diameter (MVD) of $20\text{ }\mu\text{m}$, for $t = 60\text{ min}$. Figure 4 shows the accreted ice shapes obtained from FENSAP-ICE at three different temperatures, on different sections of the blade.

4. Analyses

Results showed that variation in atmospheric temperature not only affects the shape of accreted ice, but also changes surface area covered by the ice. For $T = -2.5\text{ }^{\circ}\text{C}$, at blade tip section (Section E) the area covered by the ice is less than the iced area at $T = -15\text{ }^{\circ}\text{C}$. The effects of temperature variation is considerable near the blade tip area, whereas near the root section the ice growth is almost similar for all the temperatures. At $T = -2.5\text{ }^{\circ}\text{C}$, the ice shape at leading edge near the tip section E is more abrupt as compared to the ice shape at $T = -15\text{ }^{\circ}\text{C}$. But moving from tip to root sections the effect of temperature variation is not considerable in terms of ice growth and shapes. The change in atmospheric temperature is considerably affecting the area between blade tip and centre section, but from blade centre to blade root section this effect is almost negligible. Analyses were carried out to understand the ice growth along complete blade profile. Parameters such as accreted ice mass and ice thickness along the complete blade profile were analysed in this regard. Figure 5 shows the accreted ice mass and ice thickness variation at different atmospheric temperatures along the complete blade.

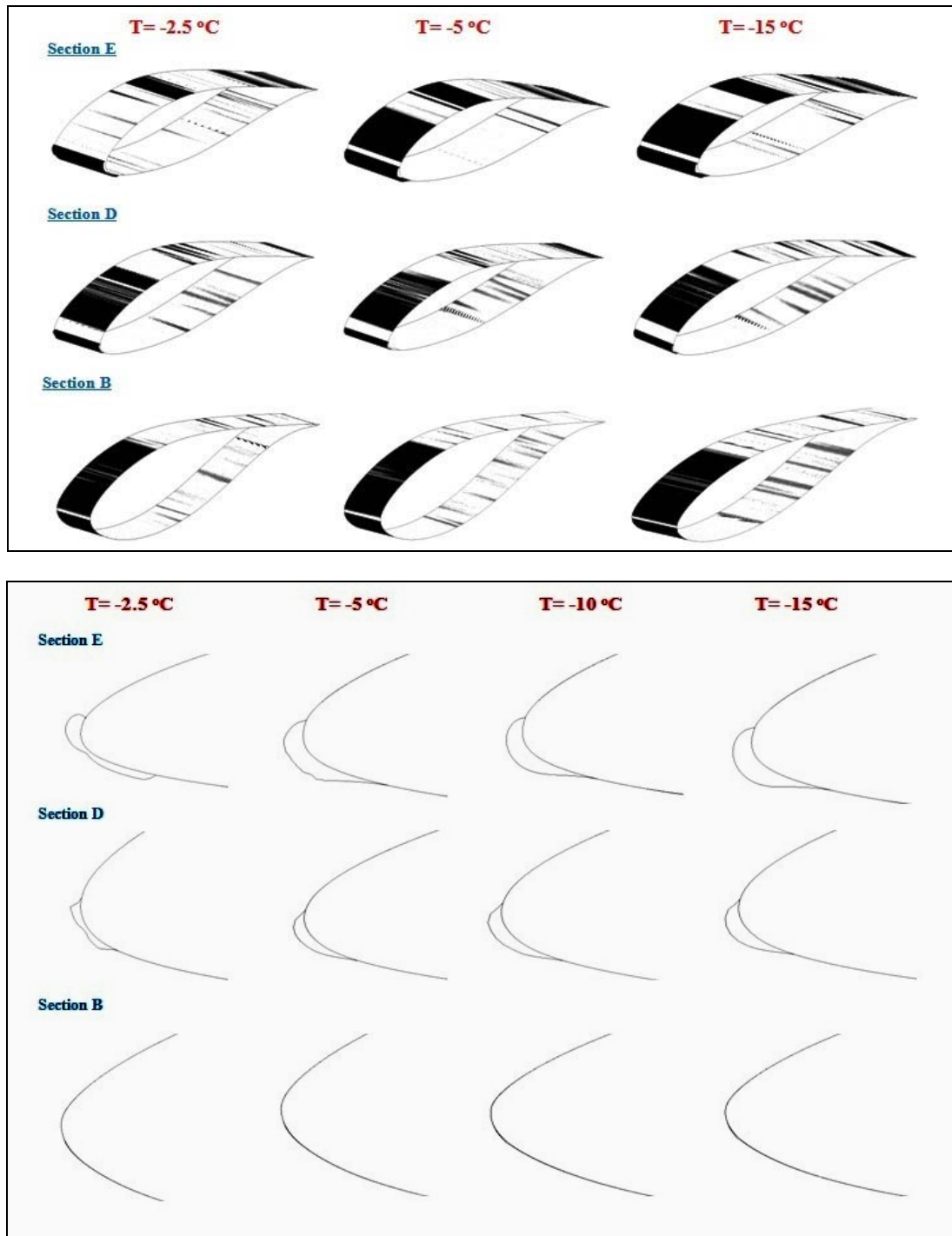


Figure 4. Effect of atmospheric temperature variation on rate and shape of ice accretion of NREL 5MW wind turbine blade (black shaded area in the figure is the area covered by the ice), $t = 60$ min

Figure 5 shows that the value of ice thickness and the accreted ice mass is maximum at the blade tip section and reduces continuously towards the root section. The most effected area of the blade by ice is from tip to the centre of the blade (from 30 m to 63 m), while rest of the area from blade centre to the blade root is not having considerable effects of icing. The trends shown in figure 5 generally agree with previous observations of more ice near the blade tips [12] and simulations with other icing codes which also show more ice near the tips [11].

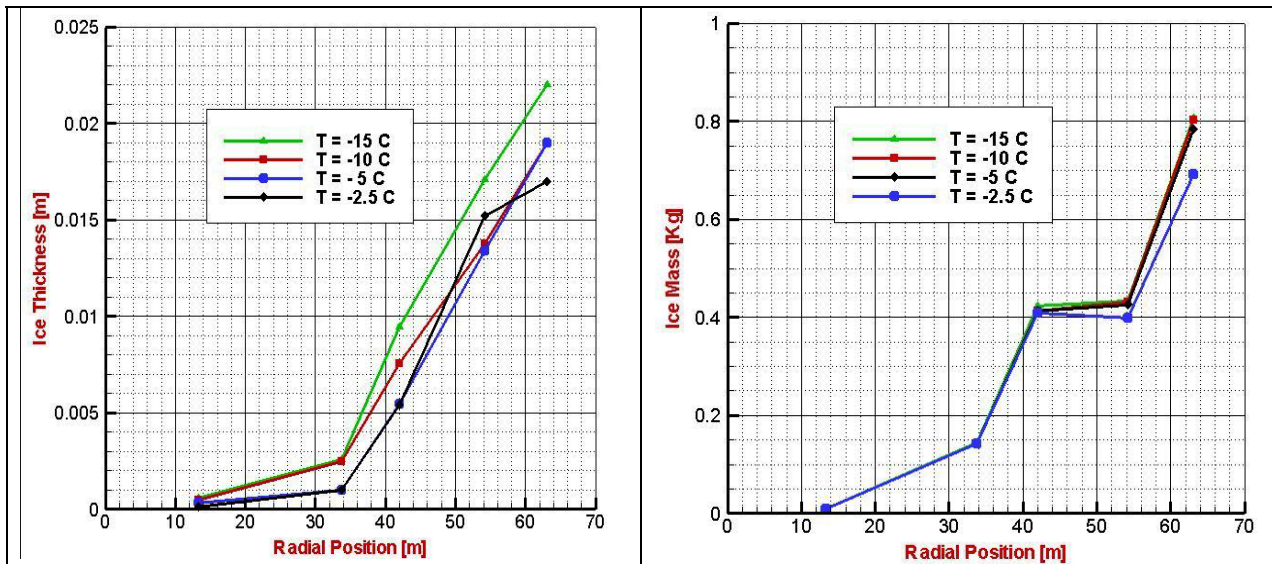


Figure 5. Effect of atmospheric temperature variation on accreted ice mass and thickness along the blade, $t = 60$ min

5. Conclusion

The rate and shape of ice accretion on a NREL 5 MW wind turbine blade was simulated using the 3D, CFD based numerical technique. The results indicate that the combined changes in blade profile size and relative velocity at each section considerably influences the ice growth. At blade sections near the tip, where the blade chord length and thickness is less, more ice accretion was found as compared to the blade sections near the root. Overall the results indicate that the icing is less severe for the blade sections, where the blade profiles are larger and thicker, both in terms of local ice mass and in terms of ice thickness. Similarly study shows that the effect of temperature variation is more significant for the blade area from tip to the centre.

These numerical analyses give rise to a number of new questions. From the results it was found that there is a considerable change in the rate and shape of ice growth with the change in geometric parameters such as chord length, blade thickness and the twist angle. It may mean that by optimizing the blade geometric parameters the ice accretion on the wind turbine blades can be minimized. This could reduce the need for de- and anti-icing systems on the wind turbine blades installed in the cold regions. Future work must include a detailed optimization study of the blade geometric parameters to minimize the ice accretion effects on the wind turbine performance.

Acknowledgements

The authors would like to acknowledge ‘Mr Nando Timmer’ from Wind Energy of Delft University of Technology for providing the blade profile coordinates of NREL 5MW wind turbine. Funding for this work was provided by Nordkraft AS and The Research Council of Norway.

References

- [1] Virk, M.S., M.C. Homola, and P.J. Nicklasson, Effect of rime ice accretion on aerodynamic characteristics of wind turbine blade profiles. *Wind Engineering*, 2010. In press.
- [2] Ronsten, G., Svenska erfarenheter av vindkraft i kallt klimat nedisning, iskast och avisning., in *Elforsk rapport 04*. 2004.
- [3] Jasinski, W.J., et al., Wind turbine performance under icing conditions. *Transactions of the ASME, Journal of solar energy engineering*, 1998. 120: p. 60-65.
- [4] Ganander, H. and G. Ronsten. Design load aspects due to ice loading on wind turbine blades. in *Proceedings of the 2003 BOREAS VI Conference*. 2003. Finnish Meteorological Institute.
- [5] John. Wind power development in sub arctic conditions with severe rime icing. in *Circumpolar climate change summit and exposition*. 2001. Whiteshore, Yukon, Canada.
- [6] Peter, D. Numerical simulation of ice accretion on wind turbines. in *IWAIS 2009*. 2009.

- [7] Tammelin, B., et al. Icing effect on power production of wind turbines. in In Proceedings of the BOREAS IV Conference. 1998. Finnish Meteorological Institute.
- [8] Marjaniemi, M. and E. Peltola. Blade heating element design and practical experiences. in In Proceedings of the BOREAS IV Conference. 1998. Finnish Meteorological Institute.
- [9] Marjaniemi, M., L. Makkonen, and T. Laakso. Turbice - the wind turbine blade icing model. in In Proceedings of the BOREAS V conference. 2000. Finnish Meteorological Institute.
- [10] Jonkman, J., S. Butterfield, and W. Musial, Defination of a 5 MW reference wind turbine for off shore system deveoplemnt. 2009, National Renewable Energy Labortary, Technical report NREL/TP-500-38060. p. 75.
- [11] Antikainen P, et al. Modelling, cerification and classification of ice loads in wind turbines. in BOREAS VI. 2003. Pyhätunturi, Finalnd.
- [12] Petteri Antikainen and S. Peuranen. Ice Loads, Case Study. in BOREAS V. 2000. Levi, Finland.
- [13] <http://www.newmerical.com/index.php/products/fensap-ice-cfd-software/>.
- [14] Manwell J F, McGowan J G, and Rogers A L, Wind Energy Explained. 2002: John Willey & Sons.
- [15] <http://wind.nrel.gov/public/jjonkman/NRELOffshrBslne5MW/>.
- [16] Shin, J., et al., Prediction of ice shapes and their effect on airfoil performance. 1991, NASA Technical Memorandum 103701.
- [17] Mortensen, K., CFD simulations of an airfoil with leading edge ice accretion, in Department of Mechanical Engineering. 2008, Technical university of Denmark. p. 117.